NANO LETTERS

Letter

pubs.acs.org/NanoLett

Controlling a Nanowire Quantum Dot Band Gap Using a Straining Dielectric Envelope

Maaike Bouwes Bavinck,*[,†] Michał Zieliński,[‡] Barbara J. Witek,[†] Tilman Zehender,[§] Erik P. A. M. Bakkers,[†,§] and Val Zwiller[†]

[†]Kavli Institute of Nanoscience, Delft University of Technology, 2600 GA Delft, The Netherlands

[‡]Instytut Fizyki, UMK, Grudziądzka 5, Toruń, 87-100, Poland

[§]Department of Applied Physics, Eindhoven University of Technology, 5600 MB Eindhoven, The Netherlands

S *Supporting Information*

ABSTRACT: We tune the emission wavelength of an InAsP quantum dot in an InP nanowire over 200 meV by depositing a SiO_2 envelope using plasma-enhanced chemical vapor deposition without deterioration of the optical quality. This SiO_2 envelope generates a controlled static strain field. Both red and blue shift can be easily achieved by controlling the deposition conditions of the SiO_2. Using atomistic empirical tight-binding calculations, we investigate the effect of strain on a quantum dot band structure for different compositions, shape, and crystal orientations. From the calculations, we estimate the applied strain in our experiment. This enables engineering of the band gap in nanowires with unprecedented possibilities to extend the application range of nanowire devices.

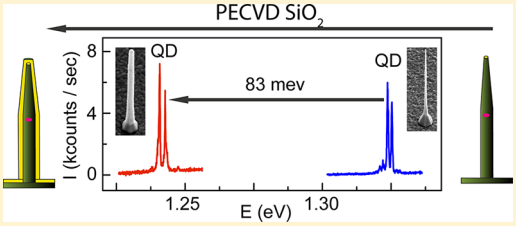

KEYWORDS: *Nanowires, quantum dots, strain, photoluminescence, band gap engineering*

Strain is a powerful parameter to control a wide range of physical properties in semiconductors. It was recently shown that strain can make direct transitions observable in germanium,[1] an indirect material when unstrained. In addition, large biaxial strain can reverse the heavy hole−light hole order with important applications in quantum communication.[2,3] Modifying the band structure with strain allows also for very large tuning ranges of frequency as shown for core−shell nanowires (NWs)[4] with applications in photon detection and light sources.[5] Additionally, strain is used to increase mobilities with tens of percentages.[6] These examples show how strain can drastically engineer the band structure of a semiconductor.

Recently, NWs have been shown to be good photon detectors[7] and can be used as single photon sources when containing a quantum dot (QD) with high light extraction efficiencies.[8] NWs allow the growth of material combinations that could not exist in bulk or thin films,[9] allowing new possibilities for the design of nanodevices. The small NW dimensions allow for band structure engineering by growing a shell of a material with different lattice constant[10] or envelope, where an envelope is grown in a different growth environment from the NW (ex situ).

Not only is the band structure engineering of NWs of interest, but also, band structure engineering of QDs has gained a lot of attention.[11,12] In particular, it is useful to shift the QDs' energy to telecom wavelength[13] or to couple the QD emission energy to another single photon emitter.[14] It is well-known that the emission energy of QDs can be altered using electric fields,[15,16] magnetic fields,[17] or temperature.[18] Using electric fields, typical red shifts in the PL are 2.5−3 μeV/mV.[19] However, the range of the shift is limited because the oscillator strength of the optical transition quenches, due to the decreasing spatial overlap of the electron−hole wave function. Also, electric fields may alter the charge state of the QD.[20] Another method to tune the quantum dot emission energy is with magnetic fields. The energy shift for III−V QDs depends on both the g-factors and the diamagnetic coefficient;[21,22] however, it usually does not exceed 100 μeV/T.[17,23] The tuning range is limited to only one direction (blue shift) and also practically limited by the available magnetic field. Yet another degree of freedom to control the band gap of the QD is the temperature. Although large modifications in the band gap can be achieved, this is of little use for QDs because high temperatures,[18] at which QDs are poor emitters, are required to obtain significant shifts.

Recently, it was shown that the band gap of QDs can be engineered using strain, for example, induced with piezoelectric actuators.[10,24] Advantages of using this technique is that both red and blue shifting are possible. Also, the method is dynamic, allowing for precise and fast tuning. However, the tuning range is limited by the breakdown of the piezo material. Today, the maximum tuning range reported is about 20 meV.[11]

Although all of these methods allow for precise tuning of the QD, the range over which the QD can be tuned is very limited. Here, we demonstrate a large tuning of the band gap of a NW−QD system using a simple SiO_2 envelope. We explore this new

Received: August 17, 2012
Revised: October 26, 2012

dx.doi.org/10.1021/nl303081m | *Nano Lett.* XXXX, XXX, XXX−XXX

technique to engineer the band gap of an InAsP QD in an InP NW. A SiO_2 envelope is deposited using plasma-enhanced chemical vapor deposition (PECVD) to generate a static strain field that can be controlled with the deposition conditions. By using photoluminescence (PL) measurements, we show that this allows tuning the emission of the QD and NW over almost 200 meV without affecting the optical quality of the QD. We show that the emission can be both blue- and red-shifted without any broadening of the linewidth. By removing the SiO_2 envelope, we recover the original NW and QD emission, showing that this technique is reversible. Using atomistic empirical tight-binding (TB) calculations, we estimate the strain and study the behavior of the band structure for different QD shapes and compositions.

Not only is our tuning method interesting from a scientific point of view, but our method could also find its application in tuning LEDs or solar cells to desired wavelength, as our method is easily scalable and straightforward to implement.

Experimental Methods. We study bottom-up grown InP NWs containing a single InAsP QD (Figure 1a). The geometry

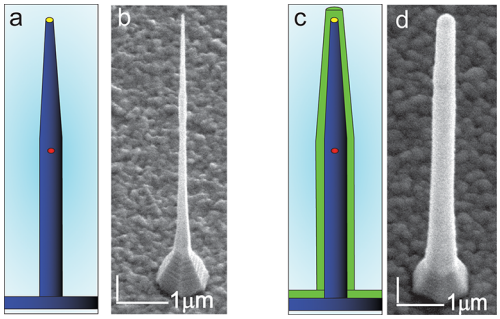

Figure 1. (a) Schematic and (b) scanning electron microscope (SEM) image of an as-grown InP nanowire (NW) with an InAsP quantum dot (QD) as-grown; (c) schematic and (d) SEM image of a NW with a SiO_2 envelope.

of the NW is controlled during growth to have a high collection efficiency: the diameter is chosen to optimize the waveguiding properties for the QD emission, and the NWs are tapered toward the top to allow an adiabatic transfer of the guided mode into free space;[25] details on the growth can be found elsewhere.[26] A typical scanning electron microscope (SEM) image of an as-grown NW can be seen in Figure 1b.

The NWs were measured in a microphotoluminescence setup at 10 K under nonresonant excitation with a laser of λ = 532 nm and a spot size of ~1 μm. The emission was collected with an objective with 0.75 NA, sent to a spectrometer, and detected with a CCD camera. The density of the NWs is 6×10^{-4} μm^{-2}, which made it possible to study single as-grown standing NWs. Marks allow measurement of the same NW before and after SiO_2 deposition.

Results. We first examine how a SiO_2 envelope deposited with the standard growth conditions influences the emission of the NW and the QD. The results are shown in Figure 2. In Figure 2a, the emission from the as-grown NW and QD (NWA) is shown. The emission detected at 1.32 eV is from the QD, and the emission at 1.40 eV is from the NW. The NW emission results from the fact that it consists of many zinc blende (ZB) and wurtzite (WZ) sections, all contributing to the PL.[27−29]

We deposit a SiO_2 envelope on NWA using PECVD. The SiO_2 was deposited at 300 °C with a silane flow of 8.5 sccm and

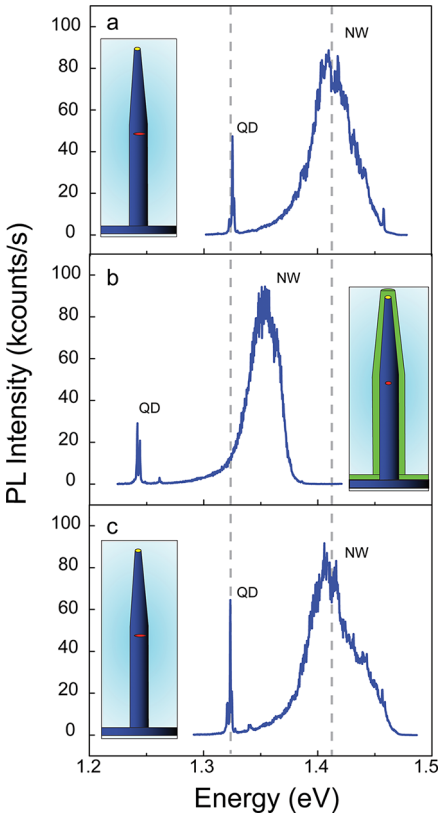

Figure 2. (a) Photoluminescence (PL) of an as-grown InP NW with an InAsP QD, (b) same NW as in (a), but now with a SiO_2 envelope. The PL is red-shifted over 59 meV for the NW and 83 meV for the QD. In (c), the SiO_2 envelope is removed, and the PL for the same NW as in (a) and (b) shifts back to its original energy.

a RF power of 20 W. The PL of NWA was measured under the same conditions after deposition of the SiO_2 envelope, and the result is shown in Figure 2b. The PL of the NW and QD is red-shifted by 59 and 83 meV, respectively. We have measured a similar shift in the PL for four different QDs and NWs (see Supporting Information).

The SiO_2 envelope can be selectively wet etched using HF. SEM images (see Supporting Information) show that the SiO_2 envelope is completely removed. Again, the PL of exactly the same NW (NWA) was measured and is shown in Figure 2c. Comparing Figure 2c with Figure 2a, it is observed that the PL has shifted back to its original value within the spectral resolution (400 μeV). As apparent from Figure 2, the SiO_2 envelope leads to large shifts of the QD and NW emission. However, to use a SiO_2 envelope to tune the QD emission wavelength, it is important that the optical quality, such as linewidth and intensity, of the QD is conserved.

From Figure 3, the linewidth of the as-grown QD (Figure 3a) and the QD with the SiO_2 envelope (Figure 3b) can be compared. Our fits to the linewidth of the exciton (X) yield the same full width at half-maximum before and after the envelope deposition. Similarly, for the biexciton (XX) line, we see no change within the spectral resolution (60 μeV).

As time-resolved measurements show that the lifetime is long (see Supporting Information), the broadening of the linewidth is attributed to fluctuating charges in the proximity of the QD.[30] Charges can, for example, be trapped in surface states[31] or impurities.[32] In NWs, surface traps are considered to be an important cause for the linewidth broadening. One would

dx.doi.org/10.1021/nl303081m | Nano Lett. XXXX, XXX, XXX−XXX

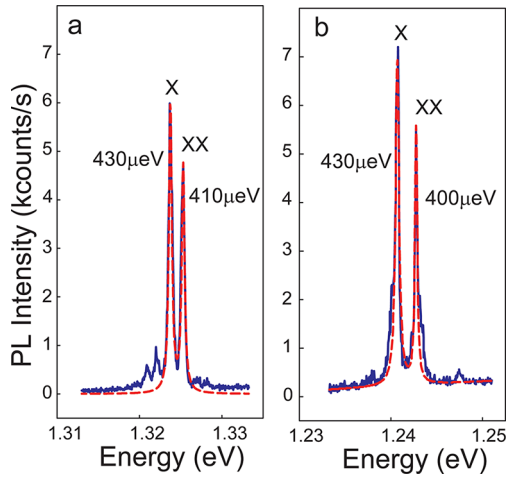

Figure 3. PL from the QD (a) before and (b) after deposition of the SiO_2 envelope. The linewidth and intensity of the exciton (X) and biexciton (XX) line are barely influenced by the SiO_2 envelope.

expect that depositing an envelope should have an effect on these surface states. We propose the following explanation for the fact that the change in the linewidth is negligible.

After the NW growth, a thin native layer of oxide is formed on the NW.[32] Surface states are then mainly expected at the interface of the InP NW and the native oxide layer.[33] As we directly grow our SiO_2 envelope without any preprocessing, the SiO_2 envelope has no direct influence on these surface states and, therefore, the charge traps will have the same contribution to the spectral broadening. Moreover, the SiO_2 envelope is amorphous and contains impurities which can serve as charge traps.[34] However, from the data, we observe that these have a negligible effect on the linewidth of the QD emission, and we conclude that these additional charge traps do not modify the QD linewidth.

Futhermore, alternating ZB and WZ segments in the NW,[27−29] called stacking faults, can trap charges which can lead to broadening of the linewidth of the QD. However, the SiO_2 envelope does not alter the number of stacking faults in the proximity of the QD, and therefore, the broadening of the linewidth due to stacking faults is expected to be minimally influenced by the SiO_2 envelope.

From Figure 3, also the intensity of the X and XX before and after deposition of a SiO_2 envelope can be compared. Although changes in the intensity were measured for QDs before and after SiO_2 deposition, no clear trend for improvement or decrease of the intensity was observed. However, the intensity with and without the SiO_2 envelope was always on the same order of magnitude.

It is possible to modify the magnitude of the QD energy shift since changing the SiO_2 deposition conditions alters the properties of the SiO_2 (see Supporting Information).[35,36] By changing the deposition conditions, one can influence the density and the percentage of H incorporation. Especially, the density has an influence on the intrinsic stress. Dense films will have a small angle between their Si−O−Si bonds leading to increased stress.[37] Figure 4 shows how changing the deposition condition alters the energy shift of the QD. In Figure 4a,c,e, three NW PL spectra are shown before the SiO_2 envelope was deposited. The SiO_2 envelope of the NW in Figure 4a (NWB) was deposited under the same growth conditions as the SiO_2 envelope of NWA by only increasing the silane flow from 8.5 to 15 sccm. Then, the PL of NWB was remeasured, and the results are shown in Figure 4b. The PL of NWB is red-shifted by 52 meV and the QD by 45 meV, which is a smaller shift compared to the deposition condition with 8.5 sccm silane flow.

A SiO_2 envelope was also deposited on the NW in Figure 4c (NWC) using again the same growth conditions as the SiO_2 envelope of NWA, but now the RF power was increased from 20 to 40 W. The results are shown in Figure 4d. The NW and QD are strongly red-shifted by 110 and 116 meV, respectively.

Figure 4f shows the PL of the exact same NW as in Figure 4e (NWD) with a SiO_2 envelope that is deposited using TEOS-PECVD, which makes use of tetraethylorthosilicate (TEOS) instead of silane to deposit SiO_2. Comparing the PL of Figure

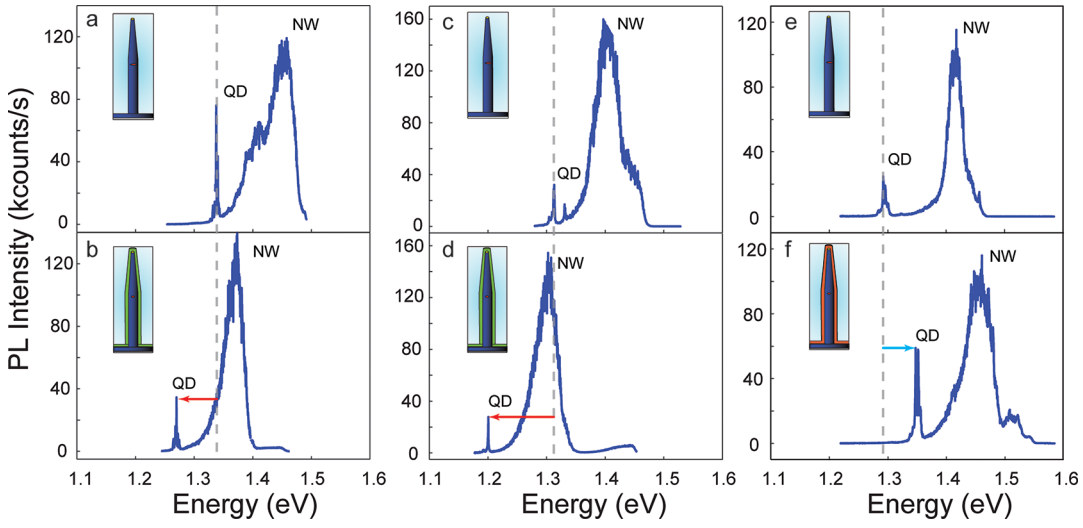

Figure 4. By changing the deposition conditions of the SiO_2 envelope, the energy of the band gap can be tuned: (a) PL of the NW before SiO_2 deposition, (b) PL of the same NW as in (a) with a SiO_2 envelope deposited with increased silane flow. The PL is red-shifted for the NW with 52 meV and for the QD with 45 meV. (c) PL of the NW before SiO_2 deposition and (d) same NW as in (c) with a SiO_2 envelope deposited with increased RF power. The PL is red-shifted for the NW over 110 and 116 meV for the QD. (e) PL before SiO_2 deposition and (f) same NW as in (e) with a SiO_2 envelope deposited with TEOS-PECVD. The PL is now blue-shifted over 55 meV for the QD and 35 meV for the NW.

dx.doi.org/10.1021/nl303081m | Nano Lett. XXXX, XXX, XXX−XXX

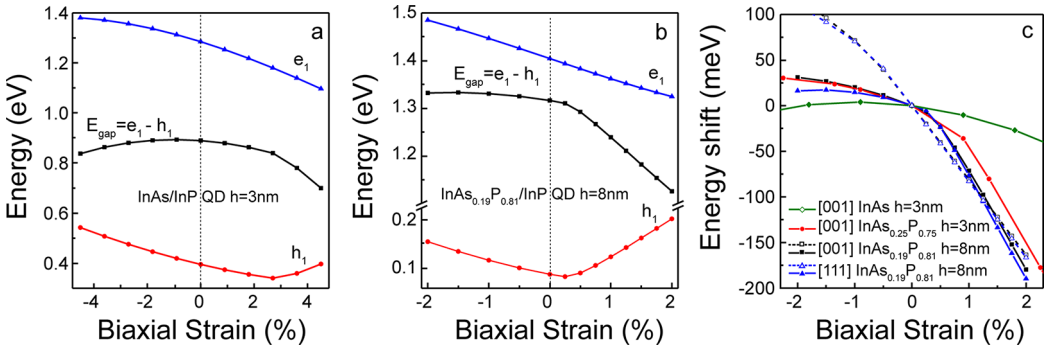

Figure 5. Evolution of the ground electron (e_1) and hole (h_1) energies and the single particle gap ($E_{gap} = e_1 - h_1$) as a function of externally applied (lateral) biaxial strain for (a) InAs/InP NW−QD of 3 nm height and (b) alloyed $InAs_{0.19}P_{0.81}$ NW−QD of 8 nm. (c) Relative energy shift compared to the unstrained system for different QD configurations. Positive values correspond to tensile biaxial strain, while negative values correspond to compressive biaxial strain. The dotted lines correspond to the pseudomorphic cylinder external strain model.

4e,f, it can be seen that the PL has now blue-shifted. The QD PL is blue-shifted by 55 meV and the NW PL by 35 meV.

From the measurements shown in Figure 4, we conclude that we can tune the band gap depending on the deposition conditions of the SiO_2 envelope. Normal SiO_2 PECVD depositon results in a decrease of the band gap, which is observed by a red shift of the PL. The shift can also be tuned: increasing the silane flow during the deposition decreases the red shift, while increasing the RF power leads to larger red shift. Increasing the band gap can be achieved by using TEOS as a reaction gas, which is observed as a blue shift in the PL.

Theoretical Calculations. These large shifts in PL can be explained by considering the effect of strain exerted by the SiO_2 envelope on the NW and the QD. We use a TB approach to calculate the electronic properties of strained NW−QDs. The SiO_2 envelope is simulated by applying external biaxial strain to the NW−QD system. As the details of the SiO_2 envelope (e.g., density, intrinsic strain) are growth-dependent[35,36] (see also Supporting Information), we vary external biaxial strain from compressive to tensile. This approach assumes a NW response in the direction perpendicular to the external strain, similar to the response to a piezoelectric actuator.[38] We also present results obtained for a model with external strain distribution similar to that in a pseudomorphic (infinitely long) cylinder.[39] Both of these simulations present an extreme case, while the real strain in the NW system is a combination of both. Relaxation of local strain (due to lattice mismatch) and applied strain (e.g., the applied strain with SiO_2 envelope) is included via atomistic valence force field theory.[40−43]

As the parameters needed for TB calculations for WZ InAs systems are under study,[44] we model the QD and NW using a ZB structure but expect our qualitative conclusions to be valid for both phases, as the two phases vary only in the position of the second nearest neighbor, while the symmetry in both systems is identical: C_{3v} for both [111]-oriented ZB and WZ. Therefore, the absolute values of the strain field should not vary significantly between the ZB [111] and WZ phases in the nearest neighbor approximation.

Here we show the results of the calculations for disk-like NW−QD of different heights and compositions. The QD is 24 nm in diameter and is embedded into the center of an InP NW of 80 nm diameter. The NW is modeled with a height of 120 nm for which the strain calculation is convergent and the single particle energies converge well below 1 meV.

The spectral properties of a non-alloyed InAs/InP QD (Figure 5a) of 3 nm height resemble that of a self-assembled InAs/InP QD with the effective gap close to 800 meV. Due to the InAs/InP lattice mismatch, the QD experiences a 3% compressive biaxial strain. Therefore, an external tensile strain of almost 3% is needed to reduce the built-in internal strain and reverse the evolution trend of the ground hole level (Figure 5a). For larger strains, the single particle gap reduces. We point out here that, despite the trend reversal, the ground hole state remains of predominantly heavy hole character due to dominant QD confinement in the vertical (growth) direction.

On the other hand, only little decrease of the effective gap is predicted for compressive biaxial strain. For larger external compressive strain, the effective gap decreases due to the dominant contribution from the ground hole state, in agreement with analogous calculation for bulk-like systems.[45]

In Figure 5b, we study the alloyed $InAs_{0.2}P_{0.8}$/InP disk-like QD of 8 nm height. Such size, shape, and composition correspond to the structural properties of the quantum dot experimentally studied in this work: the TB calculated excitonic emission is in good agreement with the observed value of ∼1.3 eV for the as-grown QD. Due to the alloying, the internal strain is reduced to a small value (∼0.5%). The lack of a significant internal strain leads to a more pronounced gap evolution with respect to the external tensile strain for an $InAs_{0.2}P_{0.8}$/InP system. Already a tensile biaxial strain on the order of 0.75% is sufficient to induce a ∼50 meV red shift of the single particle gap, while 2% tensile strain red shifts the emission peak by almost 200 meV. However, in the compressive strain regime, we again notice a small gap variation due to the cancelation of the electron and hole contributions.

The optical gap observed in the experiment is dominated by the contribution from the single particle gap but is also reduced by the electron−hole Coulomb attraction. We thus calculated the electron−hole Coulomb integral for electron and hole in their ground states for the considered $InAs_{0.2}P_{0.8}$ QD system. We found this value to be close to 16 meV and not varying significantly with the external strain within the considered strain magnitudes.

In Figure 5c, we study the relative excitonic emission peak shift as a function of externally applied strain for several systems of different size and composition. The reference point matches the emission at zero external strain for each of the considered systems. As expected from the previous analyses, NW−QD systems with larger arsenic content reveal a smaller shift of the effective gap under external tensile strain due to the countering action of the internal strain. We also investigate the effect of strain for different crystal orientations: [001] and [111]. For

dx.doi.org/10.1021/nl303081m | Nano Lett. XXXX, XXX, XXX−XXX

tensile strain, there is little quantitative difference between the two considered crystal orientations. However, for compressive strain, there is a noticeable difference between the two orientations due to different deformation potential values for large compressive [111] and [001] strains.[44]

In Figure 5c, results obtained for an external strain model assuming strain distribution similar to that in an infinitely long cylinder are shown for an 8 nm $InAs_{0.19}InP_{0.81}$ QD. Both models agree well for tensile strain, yet there is a pronounced difference for compressive strain.

The experimentally observed QD red shifts can be related to ∼0.74, ∼1.1, and ∼1.35% strains for the observed 45, 83, and 116 meV shifts, respectively. For these magnitude shifts, the pseudomorphic cylinder model predicts ∼0.55, ∼1.0, and ∼1.42% strains correspondingly.

The 55 meV blue shift observed for one of the samples is related to a compressive strain with a magnitude larger than 2%, should we assume external strain distribution analogous to that in a piezoelectric actuator. However, the same shift is achieved with only 0.66% compressive strain for an infinitely long cylinder model. As the proposed models are extreme cases, the strain in the real NW system is a combination of the two models. Therefore, the real compressive strain in the NW giving the observed blue shift is between 0.66 and 2%. For the measured red shifting of the QDs, the models predict similar values of strain.

Conclusion. We have used a very simple, but powerful, method based on a SiO_2 envelope deposition to red or blue shift the NW and QD emission energy over 200 meV. Such an extreme energy shift is achieved as a result of strain acting on the NW and QD. We demonstrate that our method preserves the QD optical quality. We observe no degradation of the linewidth within our spectral resolution and no large changes in intensity. Using TB calculations, we estimated the strain and we conclude that our technique allows one to vary the strain between a maximal 2% compressive and 1.42% tensile strain.

■ ASSOCIATED CONTENT

Supporting Information

SEM image after removing the SiO_2 envelope with HF, exciton lifetime, measured stress on Si wafers, statistics on measured shifts, details TB calculations, TB calculations for InP NWs. This material is available free of charge via the Internet at http://pubs.acs.org.

■ AUTHOR INFORMATION

Corresponding Author

*E-mail: m.h.bouwesbavinck@tudelft.nl.

Funding

The work was performed with financial support from NanoNextNL, the Dutch Organization of Fundamental Research on Matter (FOM), The Netherlands Organization for Scientific Research (NWO), the European Union Seventh Framework Programme under Grant Agreement No. 265073 (Nanowiring) and the National Science Centre based on decision DEC-2011/01/D/ST3/03415.

Notes

The authors declare no competing financial interest.

■ ACKNOWLEDGMENTS

We acknowledge M. van der Krogt, G. Bulgarini, and M.E. Reimer for technical support.

■ REFERENCES

(1) Jain, J. R.; Hryciw, A.; Baer, T. M.; Miller, D. A. B.; Brongersma, M. L.; Howe, R. T. A Micromachining-Based Technology for Enhancing Germanium Light Emission via Tensile Strain. *Nat. Photonics* **2012**, *6*, 398−405.

(2) Vrijen, R.; Yablonovitch, E. A Spin-Coherent Semiconductor Photo-detector for Quantum Communication. *Physica E* **2001**, *10*, 569−575.

(3) O'Reilly, E. P. Valence Band Engineering in Strained-Layer Structures. *Semicond. Sci. Technol.* **1989**, *4*, 121−137.

(4) Montazeri, M.; Fickenscher, M.; Smith, L. M.; Jackson, H. E.; Yarrison-Rice, J.; Kang, J. H.; Gao, Q.; Tan, H. H.; Jagadish, C.; Guo, Y.; et al. Direct Measure of Strain and Electronic Structure in GaAs/GaP Core−Shell Nanowires. *Nano Lett.* **2010**, *10*, 880−886.

(5) Li, Y.; Xiang, J.; Lieber, C. M. Nanowire Electronics and Optoelectronic Devices. *Mater. Today* **2006**, *9*, 18−27.

(6) Liu, C. W.; Maikap, S.; Yu, C.-Y. Mobility-Enhancement Technologies. *IEEE Circuits Devices Mag.* **2005**, *21*, 21−36.

(7) Bulgarini, G.; Reimer, M. E.; Hocevar, M.; Bakkers, P. A. M.; Kouwenhoven, L. P.; Zwiller, V. Avalanche Amplification of a Single Exciton in a Semiconductor Wire. *Nat. Photonics* **2012**, *6*, 455−458.

(8) Borgström, M. T.; Zwiller, V.; Müller, E.; Imamoglu, A. Optically Bright Quantum Dots in Single Nanowires. *Nano Lett.* **2005**, *5*, 1439−1443.

(9) Messing, M. E.; Wong-Leung, J.; Zanolli, Z.; Koyce, H. J.; Tan, H. H.; Gao, Q.; Wallenberg, L. R.; Johansson, J.; Jagadish, C. Growth of Straight InAs-on-GaAs Nanowire Heterostructures. *Nano Lett.* **2011**, *11*, 3899−3905.

(10) Pistol, M.-E.; Pryor, C. E. Band Structure of Core−Shell Semiconductor Nanowires. *Phys. Rev. B* **2008**, *78*, 115319.

(11) Trotta, R.; Atkinson, P.; Plumhof, J. D.; Zallo, E.; Rezaev, R. O.; Kumar, S.; Baunack, S.; Schröter, J. R.; Rastelli, A.; Schmidt, O. G. Nanomembrane Quantum-Light-Emitting Diodes, Integrated onto Piezoelectric Actuators. *Adv. Mater.* **2012**, *24*, 2668−2672.

(12) Kim, H.; Shen, T. C.; Sridharan, D.; Solomon, G. S.; Waks, E. Magnetic Field Tuning of a Quantum Dot Strongly Coupled to a Photonic Crystal Cavity. *Appl. Phys. Lett.* **2011**, *98*, 091102.

(13) Marcikic, I.; De Riedmatten, H.; Tittel, W.; Zbinden, H.; Gisin, N. Long-Distance Teleportation of Qubits at Telecommunication Wavelengths. *Nature* **2003**, *421*, 509−513.

(14) Imamoglu, A.; Awschalom, D. D.; Burkard, G.; DiVincenzo, D. P.; Loss, D.; Sherwin, M.; Small, A. Quantum Information Processing Using Quantum Dot Spins and Cavity QED. *Phys. Rev. Lett.* **1999**, *83*, 4201−4207.

(15) Heller, B.; Bockelmann, U.; Abstreiter, G. Electric-Field Effects on Excitons in Quantum Dots. *Phys. Rev. B* **1998**, *57*, 6270−6273.

(16) Kim, D.; Carter, S. G.; Greilich, A.; Bracker, A. S.; Gammon, D. Ultrafast Optical Control of Entanglement between Two Quantum-Dot Spins. *Nat. Phys.* **2011**, *7*, 223−229.

(17) Witek, B. J.; Heeres, R. W.; Perinetti, U.; Bakkers, E. P. A. M.; Kouwenhoven, L. P.; Zwiller, V. Measurement of the G-Factor Tensor in a Quantum Dot and Disentanglement of Exciton Spins. *Phys. Rev. B* **2011**, *84*, 195305.

(18) Bayer, M.; Forchel, A. Temperature Dependence of the Exciton Homogeneous Linewidth in $In_{0.60}Ga_{0.40}As$/ GaAs Self-Assembled Quantum Dots. *Phys. Rev. B* **2002**, *65*, 41308(R).

(19) Alén, B.; Bickel, F.; Karrai, K.; Warburton, R. J.; Petroff, P. M. Stark-Shift Modulation Absorption Spectroscopy of Single Quantum Dots. *Appl. Phys. Lett.* **2003**, *83*, 2235−2237.

(20) Gywat, O.; Krenner, H. J.; Berezovsky, J. *Spins in Optically Active Quantum Dots*; Wiley-VCH: Weinheim, Germany, 2010; pp 71−73.

(21) Kosaka, H.; Kiselev, A. A.; Baron, F. A.; Kim, K. W.; Yablonovitch, E. Electron g-Factor in III−V Semiconductors for Quantum Communications. *Electron. Lett.* **2001**, *37*, 464−465.

(22) Quax, G. W. W. All-Optical Control of the g-Factor in Self-Assembled (In,Ga)As/GaAs Quantum Dots, Ph.D. Thesis, Eindhoven University of Technology, September 2008; pp 25−28.

(23) Kuther, A.; Bayer, M.; Forchel, A.; Gorbunov, A.; Timofeev, V. B.; Schäfer, F.; Reithmaier, J. P. Zeeman Splitting of Excitons and

Biexcitons in Single $In_{0.60}Ga_{0.40}As$/GaAs Self-Assembled Quantum Dots. *Phys. Rev. B* **1998**, *58*, R7508−R7511.
(24) Jöns, K. D.; Hafenbrak, R.; Singh, R.; Ding, F.; Plumhof, J. D.; Rastelli, A.; Schmidt, O. G.; Bester, G.; Michler, P. Dependence of the Redshifted and Blueshifted Photolumineschence Spectra of Sinlge $In_xGa_{x-1}As$/GaAs Quantum Dots on the Applied Uniaxial Stress. *Phys. Rev. Lett.* **2011**, *107*, 217402.
(25) Friedler, I.; Sauvan, C.; Hugonin, J. P.; Lalanne, P.; Claudon, J.; Gérard, J. M. Solid-State Single Photon Sources: The Nanowire Antenna. *Opt. Express* **2009**, *17*, 2095−2110.
(26) Reimer, M. E.; Bulgarini, G.; Akopian, N.; Hocevar, M.; Bouwes Bavinck, M.; Verheijen, M. A.; Bakkers, E. P. A. M.; Kouwenhoven, L. P.; Zwiller, V. Bright Single-Photon Sources in Bottom-Up Tailored Nanowires. *Nat. Commun.* **2012**, *3*, 737.
(27) Spirkoska, D.; Arbiol, J.; Gustafsson, A.; Conesa-Boj, S.; Glas, F.; Zardo, I.; Heigoldt, M.; Gass, M. H.; Bleloch, A. L.; Estrade, S.; et al. Structural and Optical Properties of High Quality Zinc-Blende/ Wurtzite Ga As Nanowire Heterostructures. *Phys. Rev. B* **2009**, *80*, 245325.
(28) Heiss, M.; Conesa-Boj, S.; Ren, J.; Tseng, H.-H.; Gali, A.; Rudolph, A.; Uccelli, E.; Pieró, F.; Morante, J. R.; Schuh, D.; et al. Direct Correlation of Crystal Structure and Optical Properties in Wurtzite/ Zinc-Blende GaAs Nanowire Heterostructures. *Phys. Rev. B* **2011**, *83*, 045303.
(29) Akopian, N.; Patriarche, G.; liu, L.; Harmand, J.-C.; Zwiller, V. Chrystal Phase Quantum Dots. *Nano Lett.* **2010**, *10*, 1198−1201.
(30) Sallen, G.; Tribu, A.; Aichele, T.; André, R.; Besombes, L.; Bougerol, C.; Richard, M.; Tatarenko, S.; Kheng, K.; Poizat, J.-Ph. Subnanosecond Spectral Diffusion of a Single Quantum Dot in a Nanowire. *Phys. Rev. B* **2011**, *84*, 041405(R).
(31) Yeo, I.; Malik, N. S.; Munsch, M.; Dupuy, E.; Bleuse, J.; Niquet, Y.-M.; Gérard, J.-M.; Claudon, J.; Wagner, E.; Seidelin, S.; et al. Surface Effects in a Semiconductor Photonic Nanowire and Spectral Stability of an Embedded Single Quantum Dot. *Appl. Phys. Lett.* **2011**, *99*, 233106.
(32) van Vugt, L. K.; Veen, S. J.; Bakkers, W. P. A. M.; Roest, A. L.; Vanmaekelbergh, D. Increase of the Photoluminescence Intensity of InP Nanowires by Photoassisted Surface Passivation. *J. Am. Chem. Soc.* **2005**, *127*, 12357−12362.
(33) Spicer, W. E.; Lindau, I; Pianetta, P.; Chye, P. W.; Garner, C. M. Fundamental Studies of III−V Surfaces and the (III−V)-Oxide Interface. *Thin Solid Films* **1979**, *56*, 1−18.
(34) Hartstein, A.; Young, D. R. Identification of Electron Traps in Thermal Silicon Dioxide Films. *Appl. Phys. Lett.* **1981**, *38*, 631−633.
(35) Tarraf, A.; Daleiden, J.; Irmer, S.; Prasai, D.; Hillmer, H. Stress Investigations of PECVD Dielectric Layers for Advanced Optical MEMS. *J. Micromech. Microeng.* **2004**, *14*, 317−323.
(36) Adams, A. C.; Alexander, F. B.; Capio, C. D.; Smith, T. E. Characterization of Plasma-Deposited Silicon Dioxide. *J. Electrochem. Soc.* **1981**, *128*, 1545−1551.
(37) Martinu, L.; Poitras, D. Plasma Deposition of Optical Films and Coatings: A Review. *J. Vac. Sci. Technol., A* **2000**, *18*, 2619−2645.
(38) Ding, F.; Singh, R.; Plumhof, J. D.; Zander, T.; Křápek, V.; Chen, Y. H.; Benyoucef, M.; Zwiller, V.; Do, K.; Bester, G.; et al. Tuning the Exciton Binding Energies in Single Self-Assembled InGaAs/GaAs Quantum Dots by Piezoelectric-Induced Biaxial Stress. *Phys. Rev. Lett.* **2010**, *104*, 067405.
(39) Grundmann, M.; Stier, O.; Bimberg, D. InAs/GaAs Quantum Pyramids: Strain Distribution, Optical Phonons and Electronic Structure. *Phys. Rev. B* **1995**, *52*, 11969.
(40) Keating, P. N. Effect of Invariance Requirements on the Elastic Strain Energy of Crystals with Application to the Diamond Structure. *Phys. Rev.* **1966**, *145*, 637−645.
(41) Martin, R. M. Elastic Properties of ZnS Structure Semiconductors. *Phys. Rev. B* **1970**, *1*, 4005−2011.
(42) Bryant, G. W.; Zieliński, M.; Malkova, N.; Sims, J.; Jaskolski, W.; Aizpurua, J. Effect of Mechanical Strain on the Optical Propeties of Quantum Dots: Controlling Exciton Shape, Orientation and Phase with a Mechanical Strain. *Phys. Rev. Lett.* **2010**, *105*, 067404.
(43) Bryant, G. W.; Zieliński, M.; Malkova, N.; Sims, J.; Jaskolski, W.; Aizpurua, J. Controlling the Optics of Quantum Dots with Nanomechanical Strain. *Phys. Rev. B* **2011**, *84*, 235412.
(44) Zanolli, Z.; Fuchs, F.; Furthmüller, J.; von Barth, U.; Bechstedt, F. Model GW Band Structure of InAs and GaAs in the Wurtzite Phase. *Phys. Rev. B* **2007**, *75*, 245121.
(45) Kadantsev, E. S.; Zieliński, M.; Hawrylak, P. Band Engineering in Nanowires: Ab Initio Model of Band Edges Modified by (111) Biaxial Strain in Group IIIA−VA Semiconductors. *Phys. Rev. B* **2012**, *86*, 085411.